JOURNAL OF MATERIALS SCIENCE 30 (1995) 1277–1282

Measurement of residual stresses in Al_2O_3/Ni laminated composites using an X-ray diffraction technique

L. HEHN, C. ZHENG, J. J. MECHOLSKY JR
Department of Materials Science and Engineering, University of Florida, Gainesville, FL 32611, USA

C. R. HUBBARD
Oak Ridge National Laboratory, High Temperature Materials Laboratory, Oak Ridge, TN 37831, USA

Using an X-ray diffraction technique, macro-residual stresses were measured in laminated composites consisting of alternating layers of α-Al_2O_3 and nickel. The in-plane thermal mismatch stresses which develop during fabrication were found to be compressive and tensile in the α-Al_2O_3 and nickel layers, respectively. The magnitude of the in-plane stresses was found to be $\approx$ 110 MPa. Models of laminate structures predict the stress state to be biaxial in the plane of the layers. However, substantial stresses were observed perpendicular to the plane of the laminate; this stress might be due to the hot-pressing procedure used to fabricate the samples. The stress on the side surface of a laminate was measured using the indentation method and the results were consistent with those obtained by the X-ray method. Three samples were heated to 700, 900 and 1000 °C, respectively, and then cooled to test the effect of stress relaxation of the residual stresses due to the thermal expansion. The heat treatments (700–1000 °C) had no effect on the measured stress states of the laminates.

1. Introduction

Tape-cast metal/ceramic laminate composites have been shown to exhibit ductile stress–strain behaviour with improved strength and toughness over monolithic ceramic matrix materials [1]. Three strengthening and toughening mechanisms have been identified: compressive residual stress, ductile phase bridging and crack renucleation. The compressive stresses in the outer layers control the size of the cracks introduced into the surface and the maximum stress of the composite. Analytical and experimental techniques have been developed to predict and measure, respectively, the residual stresses in the laminates.

On cooling down from the sintering temperatures the thermal expansion mismatch between the alumina and nickel layers causes compressive stresses to build up in the alumina layers and tensile stresses to build up in the nickel layers until yielding occurs in the nickel layers. At the onset of yielding of the nickel, the stresses build up at a reduced rate dependent on the strain-hardening rate.

Various experimental techniques can be used to measure the residual stresses, including indentation techniques, fracture-surface analysis, neutron and X-ray diffraction techniques. Indentation techniques provide an estimate of only the surface stresses [2]. Fracture-surface analysis provides an estimate of the effective residual stress. Neutron diffraction has the potential of measuring large objects and providing an accurate mapping of residual stress within the object. However, at this time, this technique is still in development. X-ray analysis offers the potential of measuring the three-dimensional stresses of laminate composites. It is relatively easy to apply and has the potential of being made portable for on-site inspection of composite structures. This paper is a report of the measurement of residual stresses in a model metal/ceramic laminate composite. The stresses identified using X-ray analysis are compared to the stresses predicted by classical laminate analysis and to surface indentation measurements.

2. Experimental procedure

2.1. Sample fabrication

Individual layers of nickel and alumina were formed by tape casting. These green body tapes were cut, stacked, and hot-pressed in a reducing atmosphere (1300 °C, 30 MPa pressure) to form laminates (20 mm × 10 mm × 3 mm). The alternating layers of α-Al_2O_3 and nickel were each $\approx$ 300 μm thick. The material composing the outer layers of the laminate was α-Al_2O_3. These layers were half the thickness of the inner layers providing symmetrical balance of the structure [1]. The identification of faces and the coordinate system used in this study are shown in Fig. 1a.

0022–2461 © *1995 Chapman & Hall*

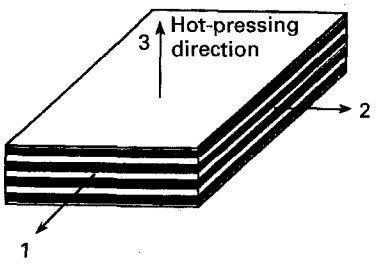

(a)

1-Face 2-Face 3-Face

$$\begin{bmatrix} -37\pm5 & -7\pm3 & -35\pm3 \\ & -114\pm8 & 5\pm6 \\ & & -74\pm8 \end{bmatrix} \begin{bmatrix} -84\pm8 & -6\pm3 & -15\pm6 \\ & -36\pm5 & -11\pm3 \\ & & -85\pm8 \end{bmatrix} \begin{bmatrix} -136\pm8 & 0\pm6 & -3\pm3 \\ & -128\pm8 & -1\pm3 \\ & & -97\pm5 \end{bmatrix}$$

(b)

$$\begin{bmatrix} -16\pm5 & 0 & 0 \\ & -95\pm8 & 0 \\ & & -115\pm8 \end{bmatrix} \begin{bmatrix} -70\pm8 & 0 & 0 \\ & -34\pm5 & 0 \\ & & -101\pm8 \end{bmatrix} \begin{bmatrix} -137\pm8 & 0 & 0 \\ & -128\pm8 & 0 \\ & & -97\pm5 \end{bmatrix}$$

(c)

Figure 1 (a) Coordinate system used to describe the stresses on the three different faces. The measured (b) and principle (c) stress tensors (MPa) [6].

2.2. Heat treatment of samples

Three samples were heated to 700, 900 and 1000 °C, respectively, at 3 °C s^{-1} and held at temperature for 1 h. The samples were cooled at 5 °C s^{-1} to 450 °C. Subsequently, the samples were removed from the furnace and allowed to cool to room temperature. It was hoped that heat treatments would cause relaxation of any stresses at temperature, and the cool-down from the different temperatures would result in different amounts of stress.

2.3. X-ray procedures

All sample surfaces were polished to a 1 μm finish with diamond paste to remove the damaged layer caused by cutting and grinding of the sample. A Scintag PTS Residual Stress Goniometer with a rotating anode X-ray source was used to make the X-ray residual stress measurements. CuK_α ($\lambda = 0.154\,059\,81$ nm) radiation was used for all the measurements with a beam spot size of approximately 3 mm diameter. Specimen tilts were made perpendicular to the diffraction plane (the so-called Chi-tilt method) which enabled tilts of up to 60° to be made without producing excessive peak broadening (detrimental to accurate peak position measurement) [3]. The use of high-angle tilts improves the precision of the strain measurements [4]. Three ϕ values of 0°, 45°, and 90° were used and χ angles were varied from +60° to −60°. The estimated error on an individual strain measurement was taken as $\pm 5 \times 10^{-5}$, based on typical reproducibility of a measurement.

To verify alignment of the diffractometer, calibration was made to NIST 640b standard silicon powder. Measurements of several peaks of the NIST standard were made at each of the tilt angles (ϕ and χ) used to make the stress measurements. The difference between the measured peak positions and the tabulated standard values was less than 0.01° 2θ for all the tilts, thus ensuring the reliability of measurements at all tilt angles.

The sensitivity to strain is highest for higher angle peaks. The X-ray beam was incident on both nickel and alumina phases on the side surfaces (1 and 2 faces). The α-Al_2O_3 (1 4 6) reflection was found to be the highest isolated peak in the two-phase pattern. The α-Al_2O_3 (1 4 6) reflection was used on the 3-face also. X-ray elastic constants for the α-Al_2O_3 (1 4 6) peak were taken from the literature [5].

Only the α-Al_2O_3 phase was measured for stress because the stress in the α-Al_2O_3 layers was considered to be the most important from the standpoint of mechanical properties of the laminates. A diagram of the coordinate systems used on the different laminate surfaces is shown in Fig. 1. The 3-face is the top surface of the laminate; the 2-face and 1-face are the sides of the laminate. In Fig. 1, the faces of the laminate are labelled by the axis which intersects the face [6]. The 3-face, for instance, is the face intersected by the 3-axis (top surface). On all faces the in-plane stresses are σ_{11} and σ_{22}.

In order to obtain unstressed lattice spacings, a powder was obtained from a piece of α-Al_2O_3 which was processed identically to that of the laminates. Measurements of relative peak intensities made on top and side surfaces showed no evidence of preferred orientation.

The mean depth of penetration is defined as the depth below the surface above which half the diffracted X-ray intensity originates. The mean depth of penetration varied from 34–13 μm for Chi tilts of 0°–60°, respectively [7, 8]. Clearly, if there are significant gradients of stress within the irradiated layer, the X-ray method produces an effective average strain.

2.4. Calculation of stresses

The strain, $\varepsilon_{\phi\chi}$ measured at an orientation defined by the angles ϕ and χ (Fig. 2) is related to the stresses, σ_{ij}, in the sample by Equation 1.

$$\begin{aligned} \varepsilon_{\phi\chi} &= \frac{d_{\phi\chi} - d_0}{d_0} \\ &= \frac{1 + \nu_{hkl}}{E_{hkl}}(\sigma_{11}\cos^2\phi + \sigma_{12}\sin 2\phi \\ &\quad + \sigma_{22}\sin^2\phi - \sigma_{33})\sin^2\chi \\ &\quad + \frac{1 + \nu_{hkl}}{E_{hkl}}\sigma_{33} - \frac{\nu_{hkl}}{E_{hkl}}(\sigma_{11} + \sigma_{22} + \sigma_{33}) \\ &\quad + \frac{1 + \nu_{hkl}}{E_{hkl}}(\sigma_{13}\cos\phi + \sigma_{23}\sin\phi)\sin 2\chi \quad (1) \end{aligned}$$

where E_{hkl} and ν_{hkl} are Young's modulus and Poisson's ratio for the given *hkl* reflection used, ϕ and χ the tilt angles, $d_{\phi\chi}$ the *d*-spacing measured at the orientation defined by the angles ϕ and χ, and d_0 the unstressed *d*-spacing.

The stresses were calculated by two different methods; the method of Dölle [10], and the

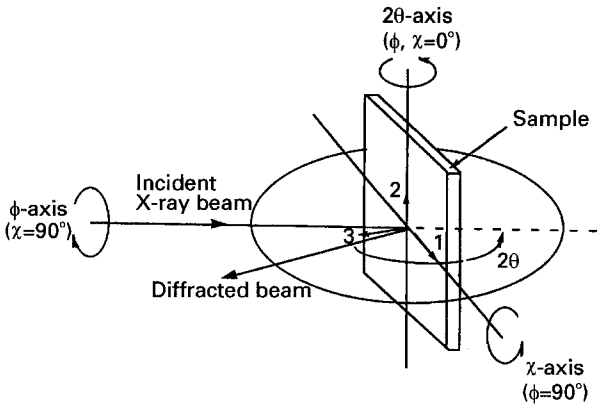

Figure 2 Diagram defining sample coordinate system and angles ϕ, χ, and 2θ. After Iancu *et al.* [9].

method of Winholz and Cohen [11]. Dölle's method involves obtaining the stresses from the slopes and intercepts of quantities a_1 and a_2 versus $\sin^2\chi$ and $\sin|2\chi|$, respectively. a_1 and a_2 are defined as

$$a_1 = \left(\frac{d_{\phi\chi+} + d_{\phi\chi-}}{2d_0} - 1\right)$$

$$= \frac{1+\nu_{hkl}}{E_{hkl}}(\sigma_{11}\cos^2\phi + \sigma_{12}\sin 2\phi + \sigma_{22}\sin^2\phi - \sigma_{33})\sin^2\chi + \frac{1+\nu_{hkl}}{E_{hkl}}\sigma_{33} - \frac{\nu_{hkl}}{E_{hkl}}(\sigma_{11}+\sigma_{22}+\sigma_{33}) \quad (2)$$

$$a_2 = \left(\frac{d_{\phi\chi+} - d_{\phi\chi-}}{2d_0}\right)$$

$$= \frac{1+\nu_{hkl}}{E_{hkl}}(\sigma_{13}\cos\phi + \sigma_{23}\sin\phi)\sin|2\chi| \quad (3)$$

where $d_{\phi\chi+}$ and $d_{\phi\chi-}$ are the d-spacings measured at tilt angles ϕ and χ, where χ^+, χ^- refer to positive and negative χ, respectively. This method is outlined in detail elsewhere [3, 10].

In Winholtz and Cohen's method, the sample stresses are recognized as being linearly related to the measured strain. If the strain is measured in at least six independent orientations, Equation 1 can be solved for the stresses (i.e. by solving six equations with six unknowns). The accuracy is improved by measuring more than six strains and employing a least squares fit of the data. The standard deviations in the stresses are obtained by propagation of the standard deviations of the individual peak fits, estimated standard deviation of the unstressed peak position, and estimated standard deviation incurred in peak position measurement through the equations used in the least squares fitting procedure. The standard deviation in the peak position measurement was estimated by making repeated measurements, moving the sample slightly each time and calculating the standard deviation of the measurements [11, 12]. The method is described in detail elsewhere [11]. The least squares fitting procedure used was incorporated into a computer program by Abuhasan [12].

3. Results and discussion

The results of the Winholz/Cohen and Dölle methods matched much better for the normal stresses, σ_{ii}, than for the shear stresses, σ_{ij}, $i \neq j$. The results from the Winholz/Cohen method are shown in Fig. 1b. The normal stresses matched within ± 2 MPa but the shears varied by up to ± 5 MPa. The variation between the two methods was random.

The shear stresses obtained from the slopes of the a_2 versus $\sin|2\chi|$ plots only consider data from $|\chi| < 45°$ 2θ because $\sin|2\chi|$ is multivalued when $|\chi|$ is allowed to exceed 45° 2θ [3]. Winholtz and Cohen's method uses all the data and is therefore more accurate. Only the stresses obtained from the latter method are presented here because it is felt that it provides increased accuracy in calculation of shear stresses. The stresses obtained from the a_1, a_2, and measured strain versus $\sin^2\chi$ plots confirmed the results of the Winholtz/Cohen least squares fitting procedure.

The strain measurements performed on all the samples indicated that the heat treatments used resulted in the same stress state, therefore the full stress analysis was performed on one sample only (700 °C anneal). Fig. 3 shows some representative plots of a_1 and strain versus $\sin^2\chi$. Because all of the plots ($\phi = 0°, 45°, 90°$) for the top surface looked the same (because $\sigma_{11} \cong \sigma_{22}$), only the strain versus $\sin^2\chi$ at $\phi = 90°$ plot is shown; likewise, because both side faces yielded very similar results, only the a_1 versus $\sin^2\chi$ plots at $\phi = 0°$ and 90° for the 1-face are shown. Data were also taken at $\phi = 45°$ but the plot is not shown because it merely gives information intermediate between $\phi = 0°$ and 90°.

TABLE I

	α-Al_2O_3	Nickel
Reflection used	(1 4 6)	Not applicable
Radiation used	Cu K_{α_1}	Not applicable
Young's modulus, E_{hkl}	407 GPa [14]	200 GPa [13]
Poisson's ratio, ν_{hkl}	0.23 [14]	0.312 [13]
Thermal expansion	$8.5 \times 10^{-6}\,°C^{-1}$ [15]	$13.3 \times 10^{-6}\,°C^{-1}$ [13]
Unstressed lattice spacing, d_0	0.083 054 6 nm (136.085° 2θ)	Not applicable
Reflection used	(1 4 6)	Not applicable
Radiation used	Cu K_{α_1}	Not applicable
χ-tilts used	0°, ±25.7°, ±37.8°, ±48.6°, ±60°	Not applicable
ϕ-tilts used	0°, 45°, 90°	Not applicable

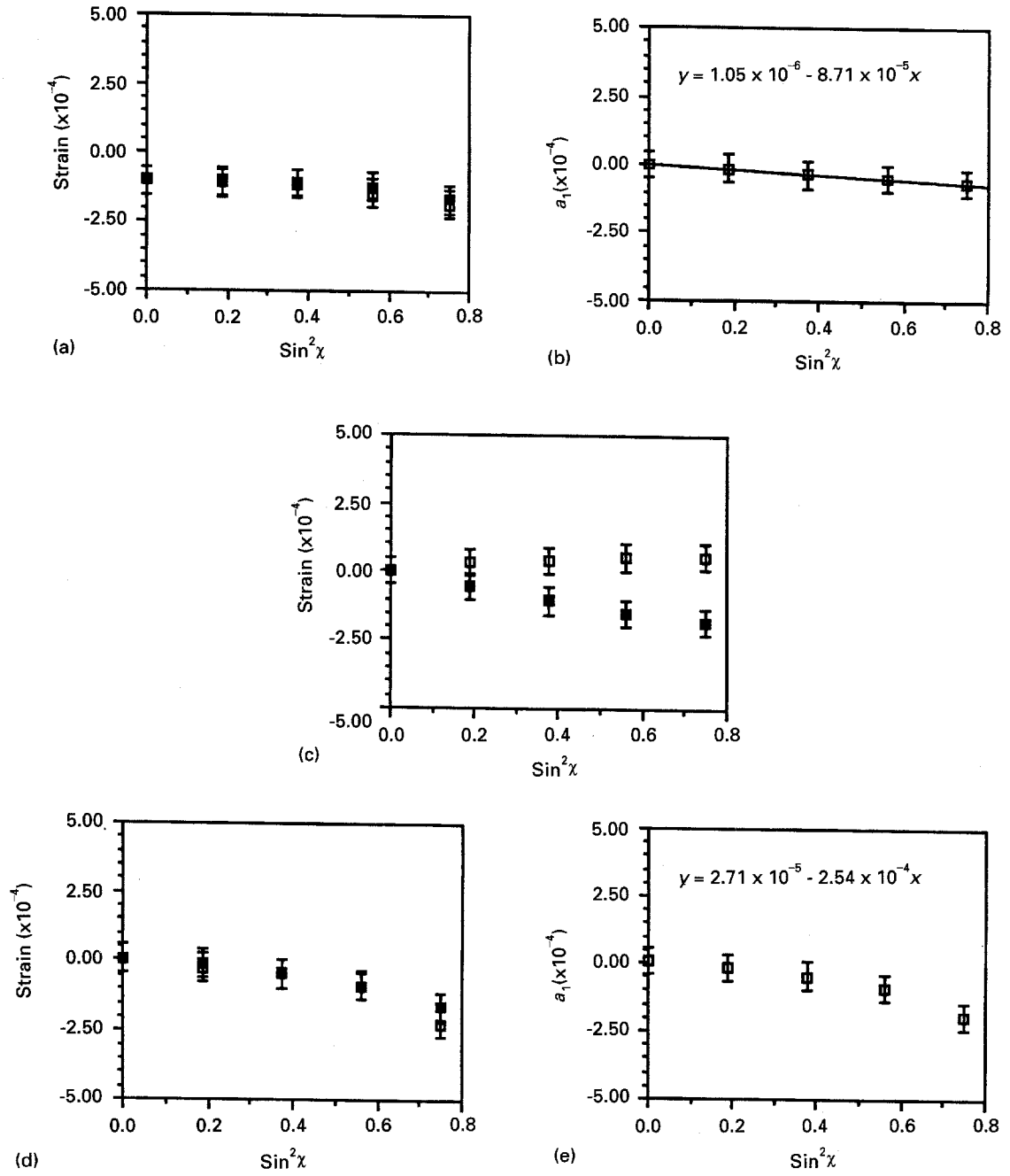

Figure 3 (a) Strain $[(d_{\phi\chi} - d_0)/d_0]$ versus $\sin^2\chi$ at $\phi = 90°$ for 3-face. (b) a_1 versus $\sin^2\chi$ at $\phi = 0°$ for 1-face. (c) Strain versus $\sin^2\chi$ at $\phi = 0$ for 1-face. (d) Strain versus $\sin^2\chi$ at $\phi = 90°$ for 1-face. (e) a_1 versus $\sin^2\chi$ at $\phi = 90°$ for 1-face. (■) χ^-, (□) χ^+.

The classical laminate analysis used in this study assumes that a plane stress condition exists in the plane of the layers (i.e. $\sigma_{33} = 0$) if the laminate structure has no curvature. If there is no curvature, then there is no force in the 3 direction and the stress in the 3 direction is zero. In qualitatively analysing the diffraction peaks, two types of strains are evident; uniform strain and non-uniform strain. If a uniform strain state exists, the diffraction peaks will be shifted from their zero strain reference positions due to a net change in d-spacing. If a non-uniform strain state exists, the diffraction peaks broaden [16]. The full-width at half-maximum (FWHM) peak widths measured on the side faces did not vary considerably from the FWHM measured on the top surface. This last result was surprising, because the X-ray beam sampled a volume containing several α-Al_2O_3 layers. Stress measurements made on the side faces can then be interpreted as being the average stress in the α-Al_2O_3 layers, as measured from the side of the laminate with the spread about this average being relatively small [17]. Measurements made on the top surface sample from one layer, as the top layer is α-Al_2O_3 and the X-ray penetration depth (13–34 μm) is much less than the layer thickness ($\simeq$ 150 μm).

The strain versus $\sin^2\chi$ plots showed splitting of the χ^+, χ^- branches (Fig. 3) for the side faces which indicated the presence of shear stresses. Except for the $\phi = 0$ plots, all of the plots of a_1 versus $\sin^2\chi$ for the side faces showed some curvature which indicated the presence of a stress gradient in one or more of the stress components over the sampling depth of the X-rays. The curvature is small however, and falls within experimental error. The measured stress tensors for

both the side faces (see Fig. 1b) contained significant shear stresses, whereas the stress tensor for the top face did not. These shear stresses are probably caused by the angle of the cut of the laminate not being exactly along a principal direction. The top face was not cut, and therefore did not contain any shear stresses. In order to compare the stresses on the different faces, all of the stress tensors were rotated into principal directions which changed the stress tensor for the top surface of the laminate slightly and significantly changed the stress tensors of the two side faces (Fig. 1c).

3.1. Comparison of stresses measured on different faces

In what follows, the stress σ_{ij} as determined from face k ($k = 1, 2$ or 3) is denoted σ_{ij}^{k}. For example, σ_{33} determined from the 1-face is σ_{33}^{1}. Loking at Fig. 1, the in-plane principal stresses (σ_{11}^{3} and σ_{22}^{3}) of the top surface (defining negative stresses as compressive) are quite close -137 and -128 MPa, respectively). It is also apparent that there is a significant σ_{33}^{3} stress (-97 MPa) which intuitively should not occur because there are no known forces acting in the direction perpendicular to the plane of the layers.

The σ_{11}^{1}, σ_{22}^{2}, and σ_{33}^{3} principal stresses must meet the condition of vanishing stress at the surface and may therefore be reduced. The fact that they are not zero is a result of the averaging of stresses over the depth of penetration. In fact, the existence of stress components normal to the surface has been shown in X-ray residual stress studies of ceramics [6, 18] and even in metals [3, 4, 19, 20] where the mean depth of penetration of the X-rays was an order of magnitude lower than in this study.

Principal stresses σ_{33}^{1}, σ_{33}^{2}, and σ_{33}^{3} are all in the same direction, they are: -115, -101, and -97 MPa, respectively. σ_{33}^{3} must meet the condition of vanishing stress at the surface and is the lowest of the three. These stresses are in reasonably good agreement.

From the results of the 3-face measurements, the in-plane stresses σ_{11} and σ_{22} should be the same. σ_{11}^{2} and σ_{22}^{1} can be compared to σ_{11}^{3} and σ_{22}^{3} because all are in-plane stresses and neither must meet the condition of vanishing stress, they are -95, -70, -137 and -128 MPa, respectively. The in-plane stresses determined from the side faces are comparable but are less than those determined from the top surface. σ_{11}^{1} and σ_{22}^{2} are also in-plane stresses but both must meet the condition of vanishing stress at the interface (compare -16 MPa to -34 MPa), note how these are similar but much lower than the other in-plane stresses. It is apparent that relief of the residual stress has occurred on the side faces. This may be caused by preferential removal of the much softer nickel layers at the surface by polishing or by the diamond polishing of the Al_2O_3.

It seems likely that the σ_{33} stress measured on all surfaces is due to the hot-pressing procedure because it occurs in the hot-pressing direction. A 1 cm × 1 cm tape-cast block of Al_2O_3 hot-pressed under the same conditions as the laminates was measured for stress. A stress (σ_{33}^{1}) of -140 MPa in the hot-pressing direction was detected. The cause of the σ_{33} stress component could be differential cooling of the outer and inner areas of the specimen during cool down from the hot-pressing temperature.

3.2. Estimation of residual stress by laminate modelling

An estimate of the thermal expansion mismatch residual stresses was calculated from the equations presented by Hseuh and Evans [21]

$$\sigma_m = \left[(\alpha_c - \alpha_m)\Delta T + \frac{\sigma_y}{n}\right]\left(\frac{1}{E_m} + \frac{t_m}{t_c}\frac{1}{E_c} + \frac{1}{n}\right)^{-1} \quad (4)$$

$$\sigma_c = -\sigma_m \frac{t_m}{t_c} \quad (5)$$

where σ, α, t, ΔT, E, σ_y and n are the residual stress, thermal expansion coefficient, layer thickness, cooling temperature range, Young's modulus, metal yield stress, and work-hardening rate of the metal, respectively. The subscripts c and m refer to ceramic and metal. This model assumes the multilayered laminate can be modelled by a three-layer laminate with outside layers ceramic and the inside layer metal. The in-plane residual stress in the outside α-alumina layers was calculated to be -116 MPa [22].

3.3. Residual stress measurement using indentation

The amount of residual compression in the alumina layers can be estimated from the measurement of the change in the length of radial cracks induced by a Vickers indentor. Vickers indentations were placed in a polished side section (a side face in Fig. 1a) of the alumina layers between the surface and the first metal layer. In the absence of residual stress, the length of cracks, b, emanating from adjacent corners of the impressions should almost be equal, due to a uniform stress field. When an in-plane residual stress field exists in the alumina layers, the length of radial crack, b^*, normal to the residual compression can be related to the magnitude of the residual stress, σ_r, by [2]

$$\sigma_r = \frac{K_c - [\eta(E/H)^{1/2} P b^{*-3/2}]}{\Omega b^{*1/2}} \quad (6)$$

where Ω is a coefficient related to the residual stress field ($\Omega = 1.128$ for uniform residual stress field), K_c the apparent fracture toughness of the unstressed α-Al_2O_3, η a geometrical constant, E Young's modulus, H the hardness, and P the load [23]. The measurements yielded the result that the stress state was biaxial with an in-plane stress of $\sigma_r = -110 \pm 8$ MPa. This result is in reasonable agreement with the σ_{11} and σ_{22} stresses in the 3-face measurement using X-ray analysis.

4. Conclusions

The stress state of the laminates was found to be triaxial instead of the biaxial state predicted by models. This was verified by measurements made on three

different faces of the laminates. Indeed, this points out perhaps the greatest advantage of the X-ray technique; the ability to measure triaxial stress states. Heat treatments made prior to making stress measurements in order to examine the effect of varying the cool-down temperature had no effect on the stress state. This was probably due to the heat-treatment temperatures being less than the temperature at which the thermal stresses began to form on cooling during processing and to the lack of stress relaxation during the heat treatment.

From the lack of broadening in the diffraction peaks obtained from the sides (as compared with those obtained from the top surface) it can be concluded that the stress does not vary much (if at all) in the direction perpendicular to the plane of the layers in the individual layers of α-Al_2O_3. This permits the stress measurements made on the side faces to be interpreted as the average stress measured inside the irradiated volume, with the stress distribution about this average being narrow. Owing to the lack of broadening of the peaks obtained from measurements made on the 1-face and 2-face, the stress could be measured on this face and compared with those measured on the 3-face, even though the 1-face and 2-face measurements were, in effect, averages over several different layers.

The results of the indentation measurements (σ(biaxial) $= -110 \pm 8$ MPa) [1] and those estimates based on Equations 5 and 6 (σ(biaxial) $= -116$ MPa) matched well with the top surface measurements of the X-ray tilt method; $\sigma_{11} = -137$ MPa, and $\sigma_{22} = -128$ MPa. However, the indentation technique did not reveal the presence of a substantial σ_{33}.

The X-ray tilt technique has been shown to be an excellent technique to use in the measurement of residual stresses in laminate systems of this type. It is hoped that the techniques used in this study can be extended to the general study of residual stresses in laminated composites.

Acknowledgement

This research was sponsored by the US Department of Energy, Assistant Secretary for Conservation and Renewable Energy, Office of Transportation Technologies, as part of the High Temperature Materials Laboratory User Program under contract DE-AC05-840R21400, managed by Martin Marietta Energy Systems, Inc.

References

1. ZHENG CHEN and J. J. MECHOLSKY Jr, *J. Am. Ceram. Soc.*, in press.
2. P. CHANTIKUL, G. R. ANSTIS, B. R. LAWN and D. B. MARSHALL, *ibid.* **64** (1981) 539.
3. C. V. NOYAN and J. B. COHEN, "Residual Stress: Measurement by Diffraction and Interpretation" (Springer, New York, 1987).
4. J. B. COHEN, H. DÖLLE and M. R. JAMES, "Stress Analysis from Powder Diffraction Patterns", National Bureau of Standards Special Publication **567** (National Bureau of Standards, Gaithersburg, MD, 1980) pp. 453–77.
5. M. KURITA, I. IHARA and A. SAITO, *Adv. X-Ray Anal.* **33** (1990) 363.
6. P. K. PREDECKI, A. ABUSHASAN and C. BARRETT, *ibid.* **34** (1991) 643.
7. B. D. CULLITY, "Elements of X-Ray Diffraction", 2nd Edn (Addison-Wesley, Reading, MA, 1978).
8. Y. M. CHEONG and H. L. MARCUS, "Advances in Surface Treatments: Technology-Applications-Effects" Vol. 4 (Pergamon Press, New York, 1987) pp. 115–24.
9. O. IANCU, D. MUNZ, B. EIGENMANN, B. SCHOLTES and E. MACHERAUCH, *J. Am. Ceram. Soc.* **73** (1990) 1144.
10. H. DÖLLE, *J. Appl. Crystallogr.* **12** (1979) 489.
11. R. A. WINHOLTZ and J. B. COHEN, *Austral. J. Phys.* **41** (1988) 189.
12. A. ABUHASAN, PhD thesis, Department of Physics, University of Denver (1990).
13. H. E. BOYER and T. L. GALL, "Metals Handbook, Desk Edition" edited by H. E. Boyer and T. L. Gall (ASM, Cleveland, OH, 1985) Sectn 1. 47.
14. A. ABUSHASAN, P. K. PREDECKI and C. S. BARRETT, *Adv. X-Ray Anal.* **31** (1988) 231.
15. E. DÖRRE and H. HÜBNER, "Alumina" (Springer, Berlin, 1984).
16. B. D. CULLITY, "Elements of X-Ray Diffraction", 2nd Edn (Addison-Wesley, MA, 1978), p. 287.
17. P. K. PREDECKI, University of Denver, personal communication, 13 April 1992.
18. L. HEHN and P. K. PREDECKI, *Adv. X-Ray Anal.* **34** (1990) 669.
19. H. DÖLLE and J. B. COHEN, *Metall. Trans.* **11A** (1980) 159.
20. I. C. NOYAN, *ibid.* **14A** (1983) 1907.
21. C. H. HSUEH and A. G. EVANS, *J. Am. Ceram. Soc.* **68**(3) (1985) 120.
22. ZHENG CHEN, MS thesis, Department of Materials Science and Engineering, University of Florida, (1992) pp. 43–44.
23. H. C. CAO and A. G. EVANS, *Acta Metall.* **37** (1989) 2969.

Received 16 December 1993
and accepted 5 September 1994